Available online at www.sciencedirect.com
ScienceDirect
Journal of Magnetic Resonance 187 (2007) 163–169
JMR Journal of Magnetic Resonance
www.elsevier.com/locate/jmr

Communication

A set of BEST triple-resonance experiments for time-optimized protein resonance assignment

Ewen Lescop, Paul Schanda, Bernhard Brutscher *

Institut de Biologie Structurale, Jean-Pierre Ebel C.N.R.S.-C.E.A.-UJF, 41, rue Jules Horowitz, 38027 Grenoble Cedex, France

Received 1 March 2007; revised 4 April 2007
Available online 13 April 2007

Abstract

A series of sequential, intra-residue, and bi-directional BEST H–N–CA, H–N–CO, and H–N–CB pulse sequences is presented that extends the BEST concept introduced recently for fast multidimensional protein NMR [Schanda et al., J. Am. Chem. Soc. 128 (2006) 9042] to the complete set of experiments required for sequential resonance assignment. We demonstrate for the protein ubiquitin that 3D BEST H–N–C correlation spectra can be recorded on a 600 MHz NMR spectrometer equipped with a cryogenic probe in only a few minutes of acquisition time with sufficient sensitivity to detect all expected cross peaks.

Keywords: Fast acquisition; Longitudinal relaxation enhancement; Resonance assignment; Selective pulses; Proteins

The sensitivity of NMR experiments is constantly increasing because of the availability of higher magnetic field magnets, cryogenically cooled probes, improved electronics, and the development of optimized NMR pulse sequences. Therefore, in many cases the acquisition times of multidimensional NMR experiments required for the study of biomolecular structure and dynamics are no longer dictated by sensitivity considerations, but by sampling requirements. The recording of a high-resolution 3D spectrum consists in the collection of several thousand scans (repetitions) resulting in acquisition times of hours up to a few days. This observation has triggered the development of new NMR data acquisition schemes yielding reduced acquisition times without loss of spectral information. Examples of fast NMR techniques proposed in recent years are non-linear time domain sampling [1,2], projection NMR [3–5], Hadamard-type [6,7] and spatial [8,9] frequency encoding, and extensive spectral aliasing [10]. These methods have in common that they rely on a reduced number of sampling points along the indirect time (or frequency) dimensions. However, most of these techniques require specific data processing algorithms in order to extract the multidimensional spectral information. An alternative to sparse data sampling is the use of short inter-scan delays to speed up data acquisition. The sensitivity (signal to noise per unit time) of such *fast-pulsing* NMR experiments can be significantly increased by longitudinal relaxation enhancement techniques [11–13], by Ernst-angle excitation [14,15], or by polarization sharing [16]. Recently, we have introduced SOFAST-HMQC [17–19], and BEST-HNCO/CA [20] experiments that allow recording of 2D ^{1}H–^{15}N and 3D ^{1}H–^{15}N–^{13}C correlation spectra of proteins within a few seconds (2D) or minutes (3D). Here, we present the extension of the BEST concept to the complete series of sequential, intra-residue, and bi-directional H–N–C ($C = CO$, C^{α}, or C^{β}) sensitivity-enhanced correlation experiments for sequential protein resonance assignment. We demonstrate that 3D data sets can be recorded in about 15–40 min per experiment using uniform time domain sampling. These acquisition times proved to be sufficient to detect all expected correlation peaks in the spectra of a 2 mM sample of ubiquitin recorded on a 600 MHz spectrometer equipped with a cryogenically cooled probe. The high signal-to-noise ratios obtained in these spectra (see Table 1) indicate that similar short acquisition times are feasible

* Corresponding author. Fax: +33 4 38 78 54 94.
E-mail address: Bernhard.Brutscher@ibs.fr (B. Brutscher).

1090-7807/$ - see front matter © 2007 Elsevier Inc. All rights reserved.
doi:10.1016/j.jmr.2007.04.002

Table 1
Acquisition parameters and statistics of 3D BEST H–N–C spectra recorded on a 2 mM sample of $^{13}C/^{15}N$-labeled ubiquitin on a 600 MHz spectrometer equipped with a cryogenically cooled triple-resonance probe

3D BEST experiment	SW_N/SW_C (kHz)	Number of complex points n_N/n_C	Exp. time (min)	Nb of peaks observed/ expected[a]	Relative S/N ratio
HNCO	0.772/1.2	19/25	21	69/69	100[d]
HN(CO)CA	0.772/2.0	19/30	27	69/69	37
HNCA	0.772/2.0	15/30	20	138/138	22/9 Intra/seq
HN(COCA)CB	0.772/8.0	15/50	38	65/65	20
HN(CO)CACB	0.772/8.0	15/50	36	134/134	24/14 C^α/C^β
iHNCA	0.772/2.0	19/30	28	69/69	15
iHN(CA)CO	0.772/1.2	15/25	25	65/69[b]	9
iHN(CA)CB	0.772/8.0	15/50	39	64/64	12
iHNCACB	0.772/8.0	15/50	38	133/133	13/9 C^α/C^β
HN(CA)CO	0.772/1.2	19/25	17	130/138[b]	11/5 Intra/seq
HNCACB	0.772/8.0	15/50	34	263/267[c]	19/11-8/5 Intra C^α/C^β-Seq C^α/C^β

The carrier frequencies for ^{15}N, ^{13}CO, $^{13}C^\alpha$, and $^{13}C^{\alpha,\beta}$ were set, respectively, at 118, 175, 56, and 46 ppm. The relative signal to noise (S/N) ratios were calculated from the average peak intensity in each experiment and normalized with respect to the HNCO experiment.

[a] Among the 76 residues the 3 proline and the N-terminal residues are not detected. Residues 24 and 53 have been excluded from the analysis because of extensive line broadening, as well as residue 36 for which the amide ^1H frequency is on the edge (6.15 ppm) of the excitation bandwidth chosen for the band-selective ^1H pulses.

[b] Cross-peaks with C^α of glycine residues have low intensity or are missing.

[c] Four sequential correlation peaks are missing (HN_9–CA_8, HN_9–CB_8, HN_{25}–CA_{24}, and HN_{65}–CA_{64}).

[d] The absolute average signal-to-noise ratio measured for correlation peaks in the BEST-HNCO spectrum was 800:1.

for recording BEST experiments on other small to medium-sized proteins in the millimolar concentration range. Interestingly, BEST experiments do not require any particular data processing tools.

The BEST (band-selective excitation short-transient) H–N–C experiments of Figs. 1–3 are optimized for minimal perturbation of aliphatic and water ^1H spins. This is realized by applying exclusively band-selective pulses, PC9 [21], E-BURP2, and RE-BURP [22], and pairs of broadband inversion pulses (BIP) [23] on the ^1H channel. The large amount of aliphatic and water ^1H spin polarization at the end of the BEST pulse sequence then enhances longitudinal (spin-lattice) relaxation of amide hydrogen spins via dipole–dipole interactions (NOE effects) and hydrogen exchange. More details about the BEST concept can be found in reference [20]. Fig. 1 shows BEST-HNCO, BEST-HN(CO)CA, and BEST-HN(CO)CACB pulse sequences for sequential correlation of the amide group of residue i with the CO, C^α, or C^β carbon of residue (i–1). Fig. 2 shows BEST-iHN(CA)CO, BEST-iHNCA, and BEST-iHNCACB pulse sequences for correlation of the amide group with the CO, C^α, or C^β of the same residue. The pulse sequence elements used to perform intra-residue $N \rightarrow C^\alpha$ coherence transfer have been introduced and described previously [24–27]. Finally, Fig. 3 shows BEST-HNCA, BEST-HNCACB, and BEST-HN(CA)CO pulse sequences for correlating the amide group with the CO, C^α, or C^β carbons of both the same and the preceding residue. As usual, the parentheses in the experiment name indicate a nuclear spin that is involved in the coherence transfer pathway, but not frequency labeled. Note that the CACB-type experiments can be tuned to yield correlation peaks either with only the C^β ((CA)CB-type, $\Delta_2 = 1/(4J_{CC})$), or with both the C^α and C^β carbons (CACB-type, $\Delta_2 = 1/(8J_{CC})$). The coherence transfer pathways of these BEST experiments are of the out and back type, and identical to the corresponding hard-pulse based correlation experiments that are routinely used for resonance assignment of $^{13}C/^{15}N$-labeled proteins. The only difference, besides the use of band-selective ^1H pulses, is the absence of any composite ^1H decoupling during ^{15}N and $^{13}C^{\alpha,\beta}$ transverse coherence evolution times that is generally applied to reduce relaxation-induced signal losses [28]. In BEST experiments, the signal loss arising from the perturbation of the aliphatic spin polarization by the composite ^1H decoupling would counterbalance the signal gain due to the longer transverse relaxation times of N_x (C_x) with respect to N_xH_z (C_xH_z) coherence. In a recent work, Diercks et al. [29] have tested and compared the performance of different broadband ^1H decoupling sequences for minimal perturbation of aliphatic ^1H polarization, and obtained the best results with an XY-16 sequence [30]. We have tested the performance of our BEST experiments using either BIP-based XY-16, band-selective IBURP-based XY-8, or no ^1H composite decoupling during the ^{15}N–^{13}C transfer periods. For ubiquitin using short interscan delays ($t_{rec} < 500$ ms), highest sensitivity was obtained for the sequences without additional ^1H decoupling (data

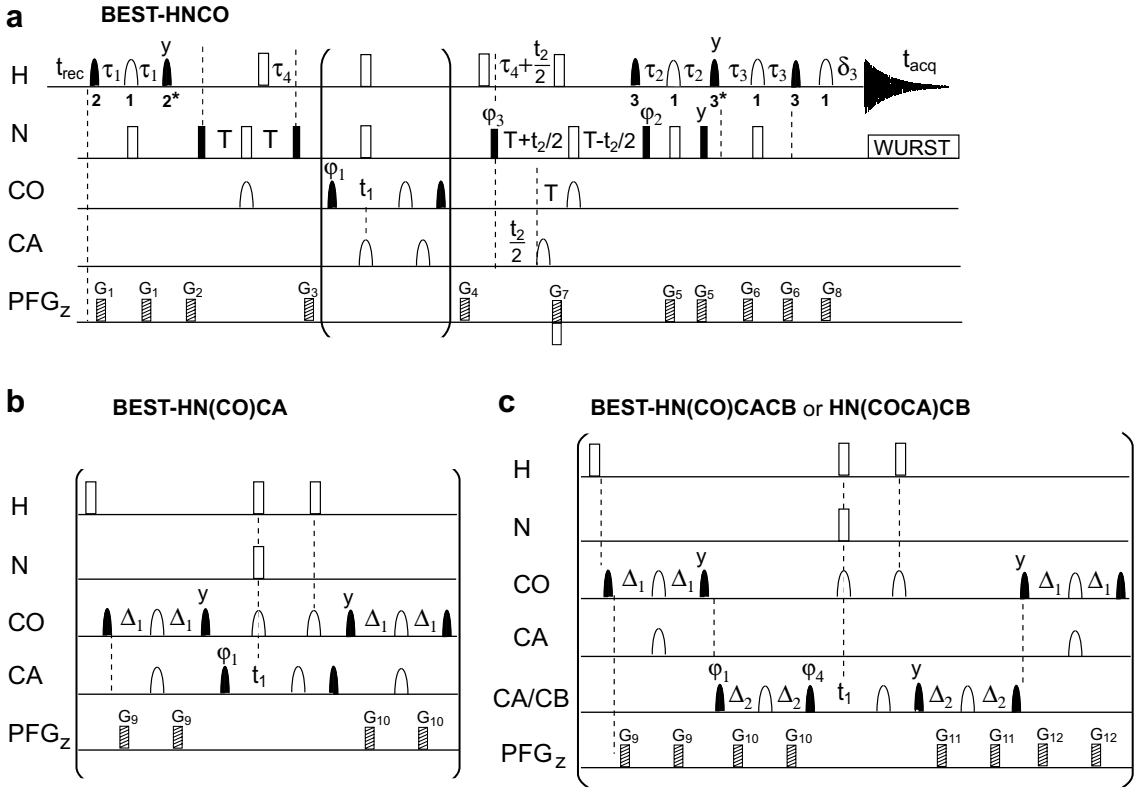

Fig. 1. BEST pulse sequences to record sequential correlation spectra of proteins: (a) BEST-HNCO, (b) BEST-HN(CO)CA, and (c) BEST-HN(CO)CACB and BEST-HN(COCA)CB. The four experiments differ by the sequence elements represented inside brackets. Filled and open pulse symbols indicate 90° and 180° rf pulses. Unless indicated, all pulses are applied with phase x. All selective ^{1}H pulses are centered at 8.2 ppm, covering a bandwidth of 4.0 ppm, with the following shapes: (1) REBURP [22], (2) PC9 [21], and (3) E-BURP2 [22]. The durations of these pulses are, respectively, 2, 3, and 1.92 ms at 600 MHz ^{1}H frequency. A star indicates a flip-back pulse obtained by time inversion of the excitation pulse shape. Open squares on ^{1}H indicate BIP-720-50-20 pulses [23]. CO pulses have the shape of the center lobe of a $\sin x/x$ function, whereas CA and CA/CB pulses are applied with a rectangular shape and zero excitation at the CO frequency. The delays are set to: $\tau_1 = 2.4$ ms – 0.5 δ_1; $\tau_2 = 2.4$ ms, $\tau_3 = 2.4$ ms – 0.5 δ_2; $\tau_4 = 2.7$ ms, $T = 14.5$ ms, $\Delta_1 = 4.5$ ms, $\Delta_2 = 3.5$ ms for CACB-type or $\Delta_2 = 7.1$ ms for (CA)CB-type experiments. The delays δ_1, δ_2, and δ_3 correspond to the pulse lengths of the PC9, E-BURP2, and G_8 gradient, respectively. These settings do not take into account the durations of the 180° rf pulses applied during the transfer delays that need to be subtracted. Pulsed field gradients, G_1–G_8 are applied along the z-axis (PFG$_z$) with durations of 200 μs–2 ms and field strengths ranging from 5–40 G/cm. The phase cycling is: $\varphi_1 = x, -x$, $\varphi_2 = x$, $\varphi_3 = 2(x), 2(-x)$, $\varphi_4 = y$, and the receiver $\varphi_{rec} = -x, x, x, -x$. In the 3D applications shown here, only a two-step cycle of φ_1 and φ_{rec} is performed. The relative durations of G_7 and G_8 are given by the gyromagnetic ratios $G_7/G_8 = \gamma_H/\gamma_N$. Quadrature detection in t_1 is obtained by time-proportional phase incrementation of φ_1 and φ_4 (if present) according to TPPI-states. For quadrature detection in t_2, echo-antiecho data are recorded by inverting the sign of gradient G_7 and phase φ_2. In addition phase φ_3 is inverted for every second t_2 increment.

not shown), and therefore composite ^{1}H decoupling was omitted in the final BEST experiments. The initial coherence transfer steps for the sequential, intra-residue, and bi-directional BEST experiments are given by Eqs. (1)–(3), respectively.

$$H_z^i \xrightarrow{J_{NH}} 2H_z^i N_z^i \xrightarrow{J_{N_{C'}}, J_{NH}} 2N_z^i CO_z^{i-1} \xrightarrow{J_{C'C\alpha}} 4N_z^i CO_z^{i-1} CA_z^{i-1} \xrightarrow{\cdots} \cdots \quad (1)$$

$$H_z^i \xrightarrow{J_{NH}} 2H_z^i N_z^i \xrightarrow{J_{N_{C'}}, J_{NC\alpha}, J_{C'C\alpha}, J_{NH}} 4N_z^i CO_z^{i-1} CA_z^i \xrightarrow{\cdots} \cdots \quad (2)$$

$$H_z^i \xrightarrow{J_{NH}} 2H_z^i N_z^i \xrightarrow{J_{NC\alpha}, J_{NH}} 2N_z^i CA_z^{i-1} + 2N_z^i CA_z^i \xrightarrow{\cdots} \cdots \quad (3)$$

A special case is the BEST-iHNCO experiment of Fig. 2c for which the coherence transfer pathway is given by:

$$H_z^i \xrightarrow{J_{NH}} 2H_z^i N_z^i \xrightarrow{J_{N_{C'}}, J_{NC\alpha}, J_{NH}} 8N_z^i CO_z^{i-1} CA_z^{i-1} CA_z^i \xrightarrow{J_{C'C\alpha}} 8N_z^i CA_z^{i-1} CA_z^i CO_z^i \quad (4)$$

The BEST pulse sequences depicted in Figs. 1–3 have been implemented in the Varian Biopack, and are available from the authors upon e-mail request.

In order to compare the performance of the BEST sequences presented here with standard hard-pulse-based sequences, we have focused on the intra-residue iHN(CA)CB experiment which presents the worst-case scenario for the BEST approach because of the long transverse N → CA (~90 ms) and CA → CB (~30 ms) transfer delays involved, and the absence of ^{1}H decoupling during these periods. Series of 1D spectra were acquired as a function of the scan time (pulse sequence length plus recycle delay) for both BEST (Fig. 2b) and standard pulse sequences on a 2 mM sample of ^{13}C/^{15}N-labeled ubiquitin (pH 6.3, 25°C) on a 600 MHz spectrometer equipped with a cryogenic triple-resonance probe. For the standard pulse sequence, band-selective H^N pulses in the sequence of Fig. 2b were replaced

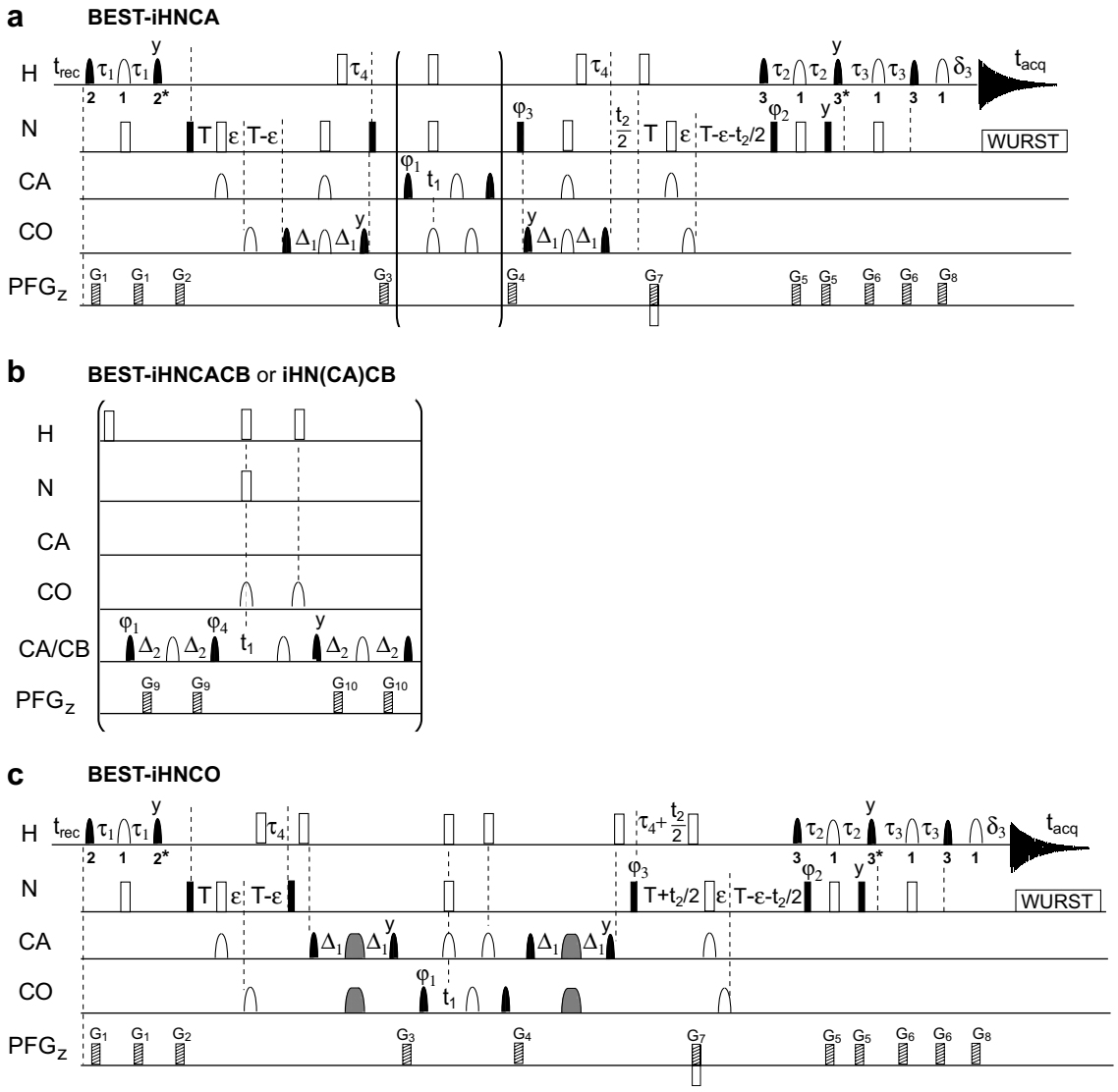

Fig. 2. BEST pulse sequences to record intra-residue correlation spectra of proteins: (a) BEST-iHNCA, (b) BEST-iHNCACB and BEST-iHN(CA)CB, and (c) BEST-iHNCO. The BEST-iHNCACB and BEST-iHN(CA)CB experiments differ from BEST-iHNCA by the sequence elements represented inside brackets. The delays and phases are identical to those given in the caption of Fig. 1, except for $T = 17$–20 ms (for sequences a and b) and $T = 22$–25 ms (for sequence c), and $\varepsilon = T$–17 ms. The grey shaped pulses applied in sequence (c) on the CA and CO channels to achieve selective CA $\rightarrow$ CO transfer are applied with a REBURP profile covering a band width of 20 ppm, and centered at 56 and 175 ppm, respectively.

by hard pulses, and additional composite ^{1}H decoupling (WALTZ-16), and water flip-back pulses were added as usual. The CA $\rightarrow$ CB transfer delays were tuned to $\Delta_2 = 1/4J_{CC}$ for complete transfer to the C$^\beta$ carbons. The 1D spectra were integrated in the range 7.2–9.5 ppm. The measured intensities normalized for equal acquisition times

Fig. 3. BEST pulse sequences to record bi-directional correlation spectra of proteins: (a) BEST-HNCA, (b) BEST-HN(CA)CO, and (c) BEST-HNCACB and BEST-HN(CA)CB. The four experiments differ by the sequence elements represented inside brackets. The delays and phases are identical to those given in the caption of Fig. 1, except for $T = 12$ ms. The grey shaped pulses applied in sequence (b) on the CA and CO channels to achieve selective CA $\rightarrow$ CO transfer are applied with a REBURP profile covering a band width of 20 ppm, and centered at 56 and 175 ppm, respectively.

Fig. 4. (a) Signal-to-noise ratio per unit of time (sensitivity) plotted as a function of the scan time T_{scan} for iHN(CA)CB spectra recorded using the BEST implementation (squares) and the standard hard-pulse version (circles). 1D spectra were recorded on ubiquitin (pH 6.3, 25 °C) at 600 MHz using a cryoprobe. The normalized intensities integrated over the range 7.2–9.5 ppm are displayed. 2D ^{1}H–^{15}N planes recorded using (c) standard, and (d) BEST versions of the iHN(CA)CB experiments were obtained with a recycle delay t_{rec} set to 200 ms ($T_{scan} = 370$ ms). The total duration of both experiments was identical ($\sim$17 min). For both experiments, 45 complex points were recorded in the ^{15}N dimension for a spectral width of 30 ppm. The acquisition times were further doubled by mirror-image linear prediction. Squared cosine apodization was applied prior to zero-filling and Fourier transformation along both dimensions. The intensity ratios obtained for individual correlation peaks are plotted in (b) versus the residue number. In addition, the secondary structural elements of ubiquitin are indicated on top of graph (b).

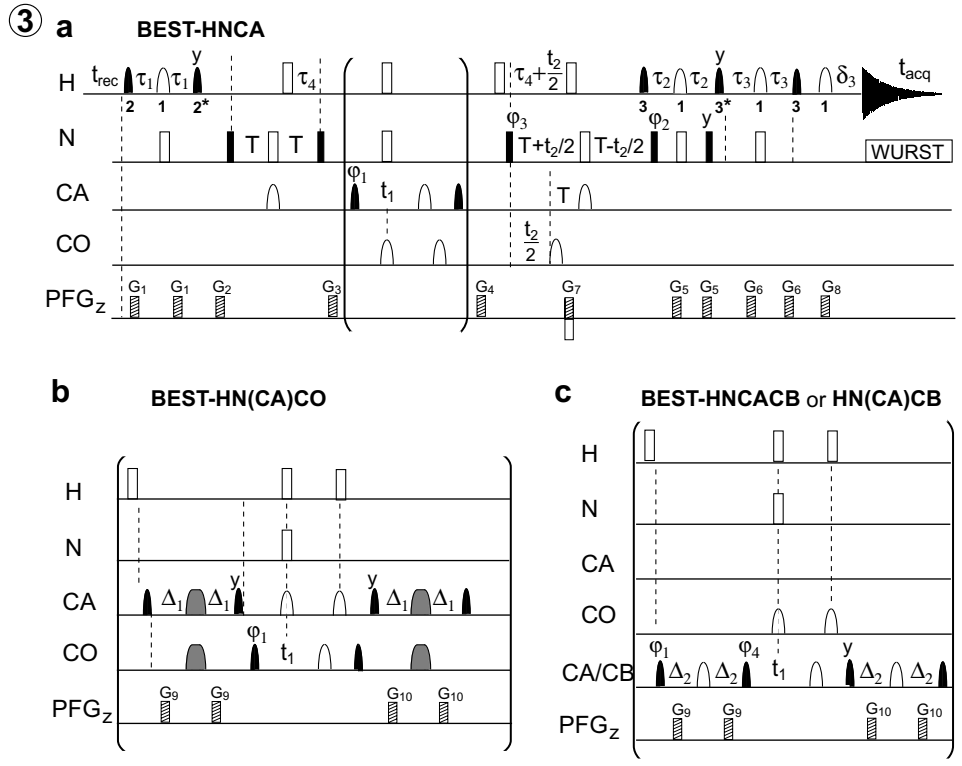
③ a
BEST-HNCA
H
N
CA
CO
PFG$_z$
WURST
b
BEST-HN(CA)CO
c
BEST-HNCACB or HN(CA)CB
CA/CB

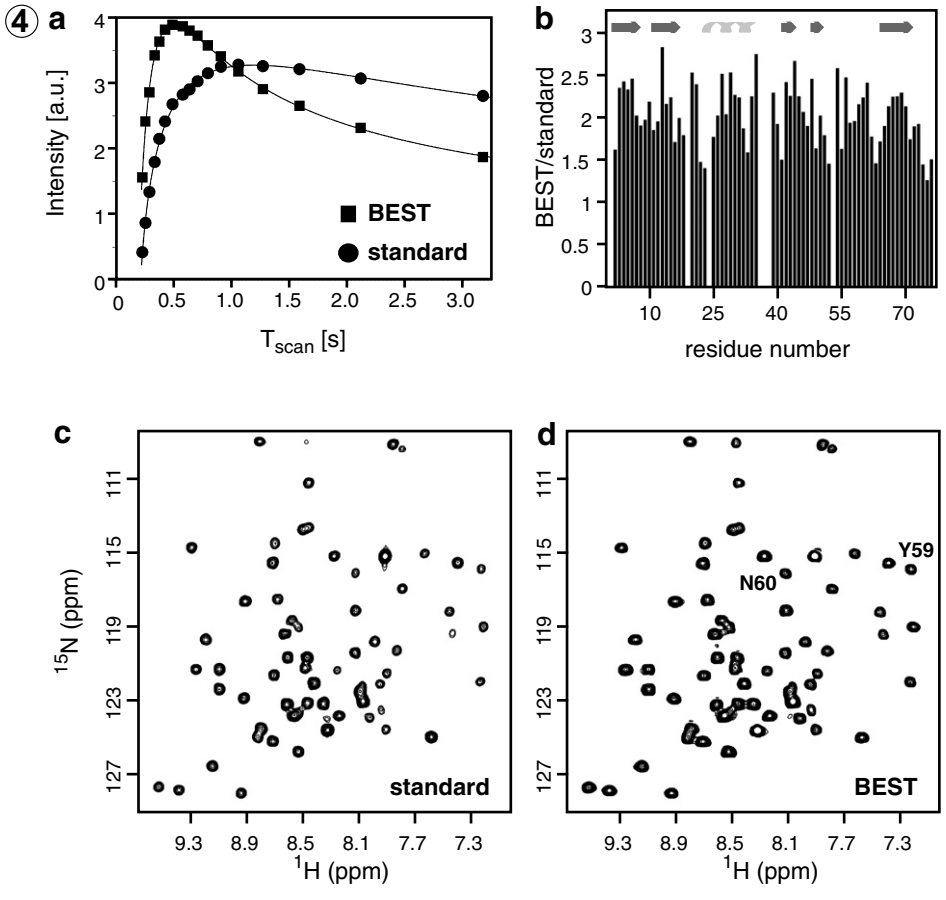
④ a
Intensity [a.u.]
T$_{scan}$ [s]
BEST
standard
b
BEST/standard
residue number
c
standard
^{15}N (ppm)
^{1}H (ppm)
d
Y59
N60
BEST
^{1}H (ppm)

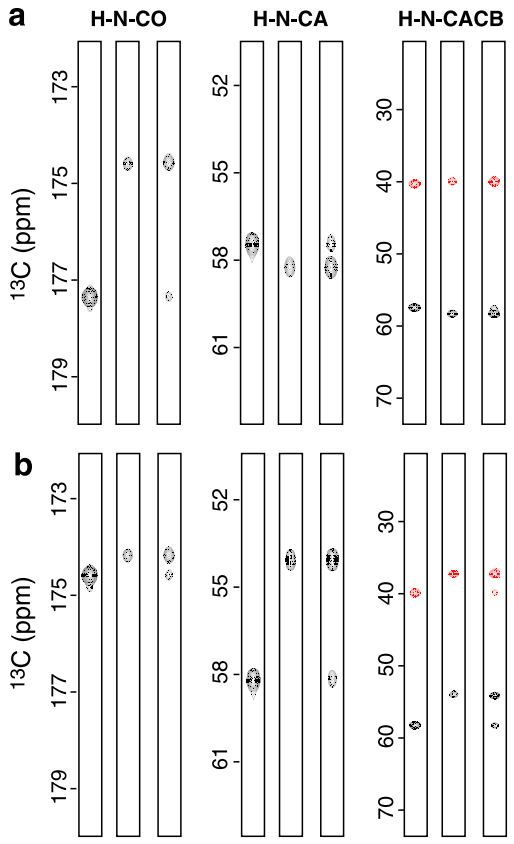

Fig. 5. $^{1}H_{N}$–^{13}C strips extracted at the $^{1}H_{N}$/^{15}N chemical shifts of residues Y59 (a) and N60 (b) from nine 3D BEST experiments used for backbone chemical shift assignment. From the left to the right: HNCO, iHNCO, HN(CA)CO, HN(CO)CA, iHNCA, HNCA, HN(CO)CACB, iHNCACB, and HNCACB. The spectra were recorded as indicated in Table 1. For data processing, linear prediction was used to extend the resolution in the ^{15}N and ^{13}C dimensions. Squared cosine apodization functions were used in all dimensions prior to zero-filling and Fourier transformation. Positive and negative correlation peaks are shown in black and grey, respectively. The spectra were plotted with the same contour levels.

are plotted as a function of the scan time (T_{scan}) in Fig. 4a. As expected from the longitudinal relaxation enhancement effect, the maximum of these sensitivity curves is shifted from $T_{scan} \approx 1.5$ s for the standard pulse sequence to $T_{scan} \approx 0.5$ s for the new BEST sequence. This results in a small absolute sensitivity gain (~25%) for the BEST experiment if optimal inter-scan delays are used for both sequences (*optimal sensitivity regime*). Higher sensitivity gains are achieved for high repetition rates of both pulse sequences. Average sensitivity gains of ~50% and ~100% are observed for scan times of 500 and 350 ms, respectively, while keeping a high overall sensitivity for the BEST experiment. Even higher gains are obtained for scan times <350 ms (*fast pulsing regime*) at the expense of a reduced overall sensitivity. Similar sensitivity curves have been obtained for a variety of other fully protonated protein samples in the <20 kDa molecular weight range (data not shown), indicating that the conclusions drawn above are also valid for larger proteins. In order to evaluate the sensitivity gain for individual amide sites along the polypeptide chain of ubiquitin we have also recorded 2D BEST-iHN(CA)CB and standard iHN(CA)CB data sets for an inter-scan delay of $t_{rec} = 200$ ms ($T_{scan} = 370$ ms). The spectra are shown in Figs. 4c and d, and a histogram of the measured intensity ratios (BEST/standard) is plotted in Fig. 4b. These data confirm the average gain of about a factor of 2 as predicted by the sensitivity curves of Fig. 4a. The sensitivity gain varies from a factor of 1.5 up to a factor of ~3.0 for individual amides, clearly demonstrating the interest of the BEST approach when high repetition rates are desired to reduce the overall experimental time required to record a complete set of 3D H–N–C correlation spectra. Even higher gains are expected for the other experiments of the BEST series.

A set of 11 3D BEST H–N–C spectra has been acquired on the 2 mM sample of $^{13}C/^{15}N$-labeled ubiquitin (pH 6.3, 25°C) on a 600 MHz spectrometer equipped with a cryogenic triple-resonance probe (see Table 1). The inter-scan delay was again set to $t_{rec} = 200$ ms for all experiments, presenting a good compromise between high sensitivity and high repetition rates. In addition, we have used ASCOM optimization [10] to minimize the ^{15}N spectral width without creating any additional peak overlap in the ^{1}H–^{15}N correlation spectrum. Using a two-step phase cycle for axial peak suppression this resulted in acquisition times ranging from 17 to 39 min per 3D experiment depending on the spectral width and resolution chosen for the ^{13}C dimension, and the available time for the CT t_2 (^{15}N) frequency labeling. The acquisition parameters, recording times, number of peaks, and the relative signal to noise ratios observed in these spectra are summarized in Table 1. The major conclusions are that all expected correlation peaks were observed in these spectra, except for four missing sequential correlation peaks in the HNCACB spectra. The undetected cross peaks in the BEST-iHN(CA)CO and BEST-HN(CA)CO spectra involve glycine residues for which the C^{α} chemical shift evolution is not refocused by the band-selective 180° pulses applied during the CA → CO transfer steps. Note that the bandwidth and carrier frequency of the amide ^{1}H pulses need to be adjusted to cover the complete chemical shift range of a given protein. Amide ^{1}H chemical shifts at the edge or outside the chosen excitation bandwidth will result in weak or absent cross peaks for this residue. On the other hand, widening the excitation band may reduce the sensitivity of the BEST experiment because of partial perturbation of aliphatic and water protons (Fig. 5).

In summary, we have presented a set of 3D BEST H–N–C experiments that yield significantly increased sensitivity for high repetition rates with respect to standard pulse sequences. We have demonstrated that these BEST pulse sequences allow recording a complete set of 3D correlation spectra as required for sequential protein resonance assignment in only a few hours. The BEST experiments are also compatible with most sparse sampling techniques,

as illustrated here by the use of spectral compression (ASCOM). This allows a further reduction in experimental times. Short overall acquisition times are of particular relevance for unstable protein samples degrading rapidly, and for monitoring fast processes. More generally, the BEST sequences allow adjusting the acquisition times to the intrinsic sensitivity of the experimental setup (sample and spectrometer). The economized spectrometer time can then be used advantageously for other less sensitive protein samples, or for spending more time recording NMR data providing quantitative information on the protein structure and dynamics (NOEs, RDCs, relaxation rate constants, J coupling constants, etc.). We have shown recently for a fully protonated sample of the 18 kDa protein fragment SiR-FP18 [31] that the application of BEST sequences is not limited to small proteins, but it proves also advantageous for larger proteins when short overall acquisition times are desired [20]. Interestingly, even for a randomly 75% deuterated sample of SiR-FP18, the longitudinal relaxation enhancement of BEST experiments still leads to sensitivity gains compared to standard experiments [20]. We are therefore convinced that the series of BEST experiments, presented here, will find widespread application in the biomolecular NMR community.

Acknowledgments

This work was supported by the Commissariat à l'Energie Atomique, the Centre National de la Recherche Scientifique, the French research agency (ANR JC-05), and the European commission (EU-NMR: JRA1). P.S. acknowledges support from the French ministry of education, research, and technology. The authors thank Isabel Ayala for the preparation of the ubiquitin sample, and Rodolfo Rasia and Jérôme Boisbouvier for many stimulating discussions.

References

[1] D. Rovnyak, D.P. Frueh, M. Sastry, Z.Y.J. Sun, A.S. Stern, J.C. Hoch, G. Wagner, Accelerated acquisition of high resolution triple-resonance spectra using non-uniform sampling and maximum entropy reconstruction, J. Magn. Reson. 170 (2004) 15–21.
[2] D. Marion, Fast acquisition of NMR spectra using Fourier transform of non-equispaced data, J. Biomol. NMR 32 (2005) 141–150.
[3] B. Bersch, E. Rossy, J. Coves, B. Brutscher, Optimized set of two-dimensional experiments for fast sequential assignment, secondary structure determination, and backbone fold validation of C-13/N-15-labelled proteins, J. Biomol. NMR 27 (2003) 57–67.
[4] H.S. Atreya, T. Szyperski, G-matrix Fourier transform NMR spectroscopy for complete protein resonance assignment, Proc. Natl. Acad. Sci. USA 101 (2004) 9642–9647.
[5] E. Kupce, R. Freeman, Projection-reconstruction technique for speeding up multidimensional NMR spectroscopy, J. Am. Chem. Soc. 126 (2004) 6429–6440.
[6] E. Kupce, T. Nishida, R. Freeman, Hadamard NMR spectroscopy, Prog. NMR Spectrosc. 42 (2003) 95–122.
[7] B. Brutscher, Combined frequency- and time-domain NMR spectroscopy. Application to fast protein resonance assignment, J. Biomol. NMR 29 (2004) 57–64.
[8] L. Frydman, A. Lupulescu, T. Scherf, Principles and features of single-scan two-dimensional NMR spectroscopy, J. Am. Chem. Soc. 125 (2003) 9204–9217.
[9] Y. Shrot, L. Frydman, Single-scan NMR spectroscopy at arbitrary dimensions, J. Am. Chem. Soc. 125 (2003) 11385–11396.
[10] E. Lescop, P. Schanda, R. Rasia, B. Brutscher, Automated spectral compression for fast multidimensional NMR and increased time resolution in real-time NMR spectroscopy, J. Am. Chem. Soc. 129 (2007) 2756–2757.
[11] K. Pervushin, B. Vogeli, A. Eletsky, Longitudinal H-1 relaxation optimization in TROSY NMR spectroscopy, J. Am. Chem. Soc. 124 (2002) 12898–12902.
[12] S. Hiller, G. Wider, T. Etezady-Esfarjani, R. Horst, K. Wuthrich, Managing the solvent water polarization to obtain improved NMR spectra of large molecular structures, J. Biomol. NMR 32 (2005) 61–70.
[13] S. Cai, C. Seu, Z. Kovacs, A.D. Sherry, Y. Chen, Sensitivity enhancement of multidimensional NMR experiments by paramagnetic relaxation effects, J. Am. Chem. Soc. 128 (2006) 13474–13478.
[14] R. Ernst, G. Bodenhausen, G. Wokaun, Principles of Nuclear Magnetic Resonance in One and Two Dimensions, Oxford University Press, Oxford, 1987.
[15] A. Ross, M. Salzmann, H. Senn, Fast-HMQC using Ernst angle pulses: an efficient tool for screening of ligand binding to target proteins, J. Biomol. NMR 10 (1997) 389–396.
[16] E. Kupce, R. Freeman, Fast multidimensional NMR by polarization sharing, Magn. Reson. Chem. 45 (2007) 2–4.
[17] P. Schanda, B. Brutscher, Very fast two-dimensional NMR spectroscopy for real-time investigation of dynamic events in proteins on the time scale of seconds, J. Am. Chem. Soc. 127 (2005) 8014–8015.
[18] P. Schanda, E. Kupce, B. Brutscher, SOFAST-HMQC experiments for recording two-dimensional heteronuclear correlation spectra of proteins within a few seconds, J. Biomol. NMR 33 (2005) 199–211.
[19] J. Losonczi, E. Kupce, G. Gray, P. Sandor, B. Brutscher, Aligning ultrafast NMR spectroscopy and cold probe technology to reveal the mysteries of protein dynamics, Am. Lab. 38 (2006) 23–25.
[20] P. Schanda, H. Van Melckebeke, B. Brutscher, Speeding up three-dimensional protein NMR experiments to a few minutes, J. Am. Chem. Soc. 128 (2006) 9042–9043.
[21] E. Kupce, R. Freeman, Wide-band excitation with polychromatic pulses, J. Magn. Reson. A 108 (1994) 268–273.
[22] H. Geen, R. Freeman, Band-selective radiofrequency pulses, J. Magn. Reson. 93 (1991) 93–141.
[23] M.A. Smith, H. Hu, A.J. Shaka, Improved broadband inversion performance for NMR in liquids, J. Magn. Reson. 151 (2001) 269–283.
[24] B. Brutscher, Intraresidue HNCA and COHNCA experiments for protein backbone resonance assignment, J. Magn. Reson. 156 (2002) 155–159.
[25] D. Nietlispach, Y. Ito, E.D. Laue, A novel approach for the sequential backbone assignment of larger proteins: selective intra-HNCA and DQ-HNCA, J. Am. Chem. Soc. 124 (2002) 11199–11207.
[26] D. Nietlispach, A selective intra-HN(CA)CO experiment for the backbone assignment of deuterated proteins, J. Biomol. NMR 28 (2004) 131–136.
[27] H. Tossavainen, P. Permi, Optimized pathway selection in intra-residual triple-resonance experiments, J. Magn. Reson. 170 (2004) 244–251.
[28] A. Bax, M. Ikura, L.E. Kay, D.A. Torchia, R. Tschudin, Comparison of different modes of 2-dimensional reverse-correlation NMR for the study of proteins, J. Magn. Reson. 86 (1990) 304–318.
[29] T. Diercks, M. Daniels, R. Kaptein, Extended flip-back schemes for sensitivity enhancement in multidimensional HSQC-type out-and-back experiments, J. Biomol. NMR 33 (2005) 243–259.
[30] T. Gullion, D.B. Baker, M.S. Conradi, New, compensated Carr–Purcell sequences, J. Magn. Reson. 89 (1990) 479–484.
[31] N. Sibille, M. Blackledge, B. Brutscher, J. Coves, B. Bersch, Solution structure of the sulfite reductase flavodoxin-like domain from *Escherichia coli*, Biochemistry 44 (2005) 9086–9095.